Original Article
cnj.araku.ac.ir

☑ Cite This: Colloid Nanosci. J. 3(3) (2025) 682-695 DOI: 10.61882/CNJ.3.3.682

Investigation of the effect of *Laurus nobilis* extract on the photocatalytic and antioxidant activity of cerium oxide

Reza Zarei Moghadam**, Hasti Samadi, Zia Rostam

Department of Physics, Faculty of Science, Arak University, Arak, Iran

ARTICLE INFO

Article History:
Received 2025-10-15
Revised 2025-12-26
Accepted 2025-12-23
Published 2025-11-01

Corresponding Authors:
Reza Zarei Moghadam
Email:
r-zareimoghadam@araku.ac.ir

ABSTRACT

The development of eco-friendly nanomaterials has attracted growing interest as sustainable alternatives to conventional chemical synthesis. In this work, cerium oxide nanoparticles (CeO_2n) were synthesized via a green co-precipitation route employing *Laurus nobilis* leaf extract as a dual reducing and stabilizing agent. The choice of *L. nobilis* is motivated by its rich content of bioactive phytochemicals, particularly polyphenols and flavonoids, which are expected to influence both nanoparticle stabilization and functional activity. The as-synthesized nanoparticles were systematically characterized by X-ray diffraction (XRD), Fourier-transform infrared spectroscopy (FTIR), ultraviolet–visible (UV–Vis) spectroscopy, and field-emission scanning electron microscopy (FESEM). XRD confirmed the formation of crystalline CeO_2n with a cubic fluorite phase, while FESEM images revealed quasi-spherical and nanorod morphologies. UV–Vis spectra showed a blue-shifted absorption edge near 300 nm, indicative of quantum-size effects, with calculated band gaps inversely related to particle size. The photocatalytic activity was assessed through the degradation of methyl orange under UV irradiation, achieving degradation efficiencies of 96.5%, 47.5%, and 77.3% for samples synthesized with 5, 10, and 15 mL of extract, respectively. The nanoparticles also demonstrated significant antioxidant potential, highlighting the synergistic contribution of phytochemicals in enhancing biological activity. From a chemical engineering standpoint, this study introduces a process-oriented approach by systematically investigating the effect of *Laurus nobilis* extract concentration on the structural, optical, and photocatalytic properties of CeO_2 nanoparticles. The results demonstrate a clear structure–property–performance relationship, offering valuable insight for the optimization and scale-up of green nanoparticle synthesis.

KEYWORDS: *Cerium oxide nanoparticles, Laurus nobilis extract, Photocatalytic, Methyl orange*

1. Introduction

Green synthesis has emerged as a promising and sustainable strategy for the production of nanoparticles owing to its non-toxic, eco-friendly, and cost-effective characteristics [1-6]. Unlike conventional chemical and physical synthesis routes, which often require harsh reducing agents, toxic solvents, and high energy inputs, green synthesis utilizes biological systems such as microorganisms and plant extracts, thereby reducing environmental impact while ensuring process safety [7]. Among biological resources, plant extracts are particularly advantageous because they are widely available, inexpensive, and rich in diverse phytochemicals including polyphenols, flavonoids, alkaloids, and terpenoids that serve as natural reducing and stabilizing agents. These bioactive compounds not only facilitate nanoparticle nucleation and growth but also modulate particle morphology, crystallinity, and functional properties.

Cerium oxide nanoparticles (CeO_2n) have attracted considerable attention due to their exceptional redox behavior, oxygen storage capacity, and multi-enzyme mimetic activities. These features underpin their wide-ranging applications in catalysis, fuel cells, UV filters,

sensors, and biomedical fields [8]. Moreover, CeO_2n exhibit strong antioxidant, antibacterial, and drug delivery potential, highlighting their versatility in both environmental and healthcare sectors [9]. In particular, the photocatalytic degradation of synthetic dyes, such as methyl orange, has emerged as an important application. Industrial dye effluents are characterized by intense coloration, high stability, and poor biodegradability, posing a significant challenge to conventional treatment methods such as electrolysis, coagulation, and filtration [10]. By contrast, photocatalytic nanomaterials provide an efficient, eco-friendly, and cost-effective solution to wastewater remediation [11].

Within this context, *Laurus nobilis* (bay laurel), an aromatic Mediterranean plant traditionally valued for its culinary and medicinal uses, presents a unique opportunity for nanoparticle biosynthesis. The leaves of *L. nobilis* are enriched with polyphenols, flavonoids, tannins, and essential oils, which exhibit antioxidant, antifungal, and cardioprotective properties [12]. Such phytochemicals not only enhance the stability of nanoparticles but also synergistically contribute to their biological and catalytic performance. While several studies have explored green synthesis of CeO_2n using various plant extracts the use of *L. nobilis* has been scarcely investigated, particularly about the influence of extract concentration on nanoparticle structure, photocatalytic efficiency, and antioxidant activity. This research thus introduces a novel perspective by linking the phytochemical richness of *L. nobilis* with the tailored physicochemical and functional properties of CeO_2n.

Accordingly, the present study reports the green co-precipitation synthesis of CeO_2n using *L. nobilis* leaf extract and evaluates their structural, morphological, and functional characteristics. Special emphasis is placed on the effect of extract concentration on particle size, crystallinity, band gap, and photocatalytic degradation efficiency. Beyond demonstrating the feasibility of plant-mediated CeO_2n synthesis. From a chemical engineering perspective, the novelty of this study lies in the systematic evaluation of plant-extract concentration as a key process parameter in the green co-precipitation synthesis of CeO_2n. Rather than merely demonstrating a green synthesis route, this work establishes a clear correlation between extract dosage, nanoparticle structural evolution, optical properties, and functional performance. To the best of our knowledge, this is the first report employing *Laurus nobilis* leaf extract for the controlled synthesis of CeO_2n, while simultaneously assessing their photocatalytic and antioxidant activities. The findings provide practical insight into process optimization and highlight the potential of phytochemical-assisted synthesis for scalable and sustainable nanomaterial production.

2. Material and Methods

Cerium(III) nitrate hexahydrate ($Ce(NO_3)_3{\cdot}6H_2O$) and sodium hydroxide (NaOH), 2,2-diphenyl-1-picrylhydrazyl (DPPH), supplied by Merck, were used as precursors with a purity level of 99.99%. *Laurus nobilis* leaves were utilized for the preparation of the plant extract, which served as both a reducing and stabilizing agent in the synthesis process. All experimental procedures were conducted using double-distilled water to ensure high purity.

2.1 Extraction method

The extraction process was carried out as follows: Fresh leaves of the *Laurus nobilis* were prepared in the city of Arak, Iran. Fresh *Laurus nobilis* leaves were thoroughly washed with tap water followed by double-distilled water to remove surface contaminants. The cleaned leaves were then sun-dried for several days to eliminate moisture. Once dried, the leaves were ground into a fine, homogeneous powder using a mechanical grinder. To prepare the extract, 20 g of the powdered leaves were mixed with 100 mL of deionized water and heated to boiling under constant stirring. The mixture was then filtered using Whatman filter paper to separate the solid residue from the liquid extract. The resulting aqueous extract was stored at 4°C in a sterile container for subsequent use.

2.2. Synthesis of cerium oxide nanoparticles (CeO_2n)

The synthesis of cerium oxide nanoparticles was performed via a co-precipitation method using *Laurus nobilis* extract. Initially, 0.5 M cerium (III) nitrate hexahydrate was dissolved in 100 mL of deionized water under continuous stirring to ensure complete dissolution. Subsequently, varying volumes of the prepared *Laurus nobilis* extract (5 mL, 10 mL, and 15 mL) were added to the solution, followed by stirring for 30 minutes to facilitate the reduction and stabilization of cerium

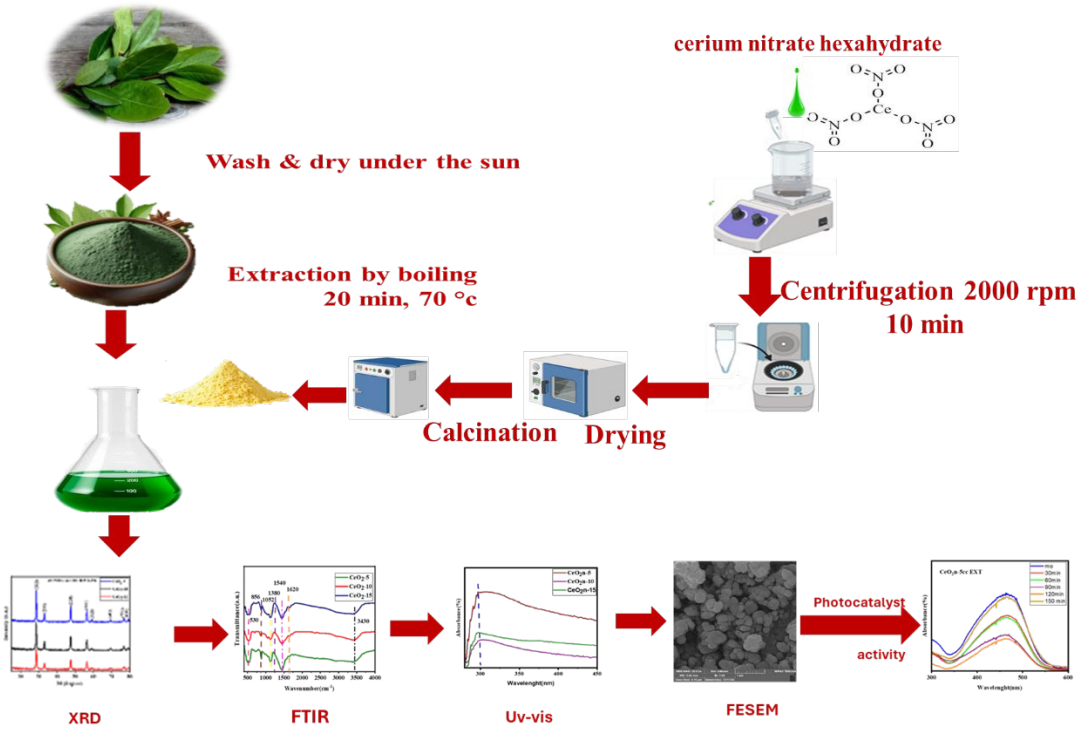

Fig. 1. Schematic representation of the extraction process, green synthesis of cerium oxide nanoparticles using *Laurus nobilis* extract.

ions. The pH of the mixture was adjusted to 10 using a sodium hydroxide solution to promote nanoparticle formation. After the reaction, the resulting suspension was centrifuged at 4000 rpm for 20 minutes to separate the nanoparticles from the supernatant. The precipitate was washed three times with deionized water to remove any unreacted species or impurities. The washed precipitate was then dried in an oven at 120°C for 6 hours to evaporate residual moisture. Finally, the dried material was calcined at 600°C for 4 hours in a muffle furnace to enhance crystallinity, yielding a light-yellow powder composed of cerium oxide nanoparticles. Figure 1. Schematic representation of the extraction process, green synthesis of cerium oxide nanoparticles using *Laurus nobilis* extract, and characterization steps including XRD, FTIR, FESEM, and UV-Vis analyses.

2.3. Characterization of samples

The chemical bonds and crystalline structure of the synthesized nanoparticles were analyzed using advanced analytical techniques. Fourier-transform infrared spectroscopy (FTIR) was performed using a Takram Pulse N1-541 spectrometer (Teksan Co.) to investigate the functional groups and bonding characteristics. X-ray diffraction (XRD) analysis was conducted on a D8-Advance diffractometer (Bruker), employing CuKα radiation, to determine the crystallinity, phase purity, and structural properties of the nanoparticles. The morphological features of the samples were examined using field emission scanning electron microscopy (FESEM) with a MIRA3 system (Tescan), providing high-resolution imaging of particle size and shape. Additionally, the optical properties of the nanoparticles were evaluated using UV-Vis spectroscopy with a Shimadzu 1800 UV-visible double-beam spectrophotometer (model 165-PC), enabling precise measurement of absorption spectra and band gap energy.

2.4. Photocatalytic process

This study investigates the photocatalytic performance of CeO_2n. elucidating the mechanisms underpinning its activity upon ultraviolet (UV) irradiation. Specifically, exposure to UV light results in the absorption of hγ energy by the CeO_2n photocatalyst, promoting electrons from the valence band to the conduction band, thereby

generating electron-hole pairs. Subsequent to this excitation, two distinct recombination pathways are posited for these photogenerated charge carriers. The initial pathway involves direct electron-hole recombination, resulting in energy dissipation and a return of the electron to the conduction band. Alternatively, electrons from the conduction band may migrate to the surface of the CeO_2n material, where they interact with adsorbed oxygen molecules present in the surrounding atmosphere. This surface reaction facilitates the reduction of molecular oxygen, leading to the formation of superoxide anion radicals ($O_2^{-}\bullet$), a key reactive oxygen species often implicated in the degradation of organic pollutants in photocatalytic applications. The relative prevalence of these two recombination pathways is expected to significantly influence the overall photocatalytic efficiency of the CeO_2n material. Figure 2 shows the mechanism of photocatalytic activity of CeO_2n.

To examine the photocatalytic effect, methyl orange was selected as the pollutant of interest. This compound is commonly utilized in the textile industry, and its presence in wastewater can lead to significant health risks. These issues encompass respiratory and gastrointestinal complications, and inhalation may also lead to irritation of the skin and eyes[13]. The degradation rate of the photocatalyst is determined using the following formula [13, 14].

$$\%\text{degradation} = \left(A_t / A_o\right) \times 100 \quad (1)$$

A_o and A_t represent the absorbance of the dye before it starts to degrade and the absorbance of the dye at a specific time "t" after degradation has occurred, respectively. This equation allows for a precise determination of the extent to which the photocatalyst has successfully broken down the methyl orange molecule over a given period, providing a crucial metric for evaluating the photocatalytic performance.

2.5. Antioxidant activity

For measurement of antioxidant activity various concentrations of CeO_2n (2.5, 7.5, 12.5 and 17.5 µg/mL) were added to 10 mL of a 0.1 mM 2,2-diphenyl-1-picrylhydrazyl (DPPH) solution and kept in complete darkness for at least 40 min at room temperature. Absorbance was recorded using ethanol as black at 517 nm wavelength. Ascorbic acid was used as the standard in all performing experiments. The antioxidant activity of green synthesized CeO_2n was evaluated by DPPH radical scavenging assay using the following formula:

$$\%\ \text{Inhibition} = \frac{\text{Absorbance of Control} - \text{Absorbance of Sample}}{\text{Absorbance of Control}} \times 100 \quad (2)$$

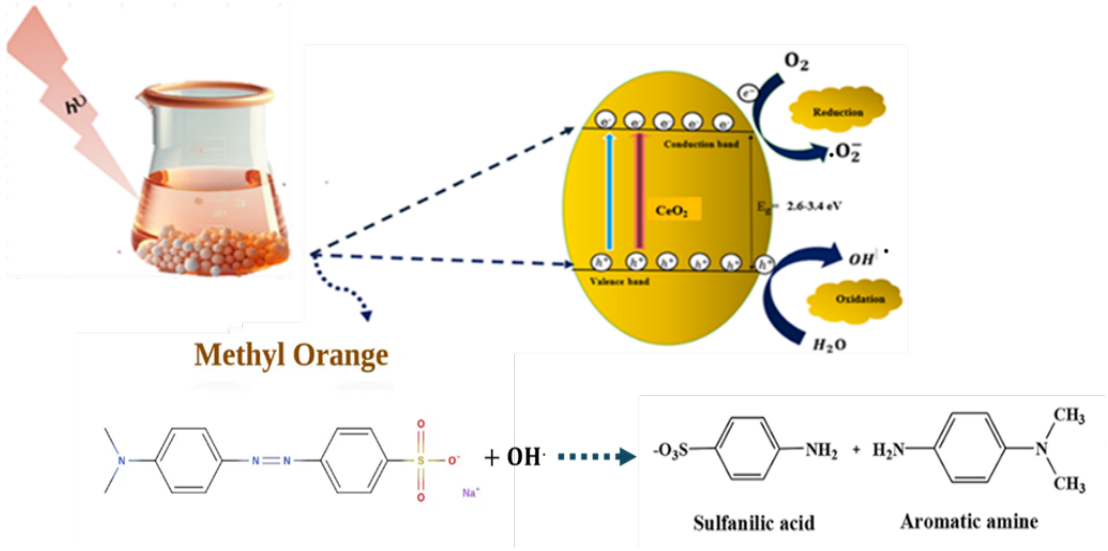

Fig. 2. Mechanism of CeO_2n photocatalytic activity.

3. Result and discussion

3.1. XRD analysis

X-ray diffraction (XRD) analysis was employed to characterize the crystalline properties of CeO_2n synthesized at three distinct concentrations, allowing for the determination of crystal structure, crystallite size, and phase purity within the 2θ range of 10° to 80°. As depicted in Figure 3, the XRD patterns for the three samples exhibited distinct diffraction peaks, with characteristic reflections observed at 2θ values of 28.6°, 33.2°, 47.6°, 58.7°, 69.6°, 77.2°, and 79°, which were indexed to the (1 1 1), (0 0 2), (0 2 2), (1 1 3), (2 2 2), (0 0 4), and (1 3 3) planes of cerium oxide, respectively. These observed diffraction patterns are consistent with the cubic fluorite structure of CeO_2n, exhibiting a high degree of similarity with the reference data provided by the JCPDS card number 8436-089-01, thus confirming the successful synthesis of crystalline CeO_2. Furthermore, analysis of the XRD data revealed an inverse relationship between the concentration of the extract used during synthesis and the resulting crystallite size, as evidenced by the decrease in particle size observed with increasing extract quantity, an observation that is congruent with findings reported in prior investigations [15]. The size of the nanocrystals was measured using the Debye-Scherrer equation [16].

$$D = \frac{K\lambda}{\beta \cos\theta} \tag{3}$$

Where D is the crystal size, K and λ (Cuk_α) are 0.9 and 1.54060 nm, respectively, and β is the peak width at half maximum (FWHM) [17]. The results of the Debye-Scherrer equation indicate that the size of the cerium oxide nanocrystals at a 5 mL extract concentration is 21.11 nanometers, at a 10 mL concentration is 16.1 nanometers, and at a 15 mL concentration is 15.53 nanometers. The observed inverse relationship between extract concentration and nanocrystal size suggests that the extract plays a significant role in controlling nanocrystal growth. As the concentration of the extract increases, it likely introduces more binding or capping agents to the developing nanocrystals, hindering further aggregation and ultimately resulting in smaller particle sizes. This effect may be attributed to enhanced surface stabilization or increased nucleation rates influenced by the extract's components. Numerous research groups have demonstrated the feasibility of employing plant-derived extracts as reducing and capping agents in the biosynthesis of cerium oxide

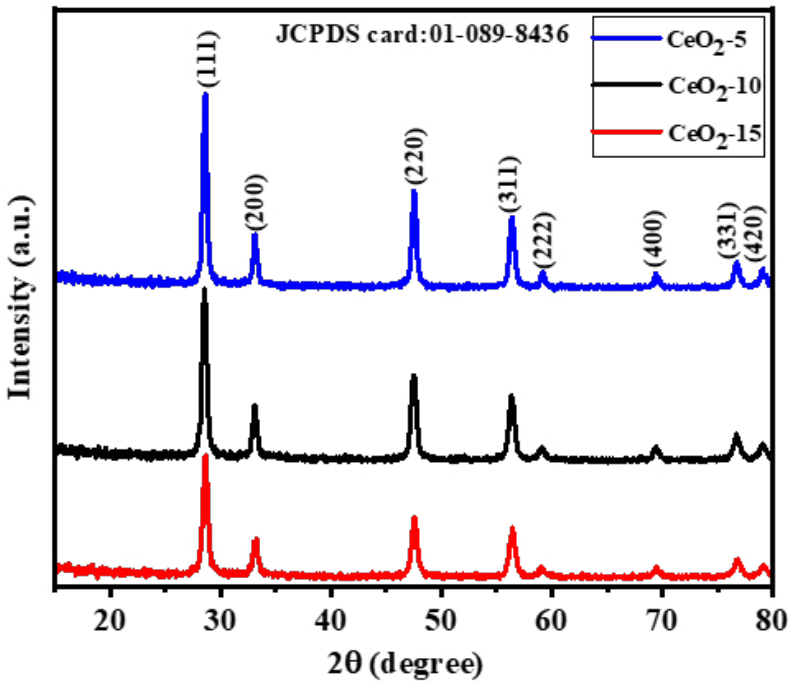

Fig. 3. X-ray diffraction pattern of CeO_2n for three samples with different concentrations of *laurus nobilis* extract.

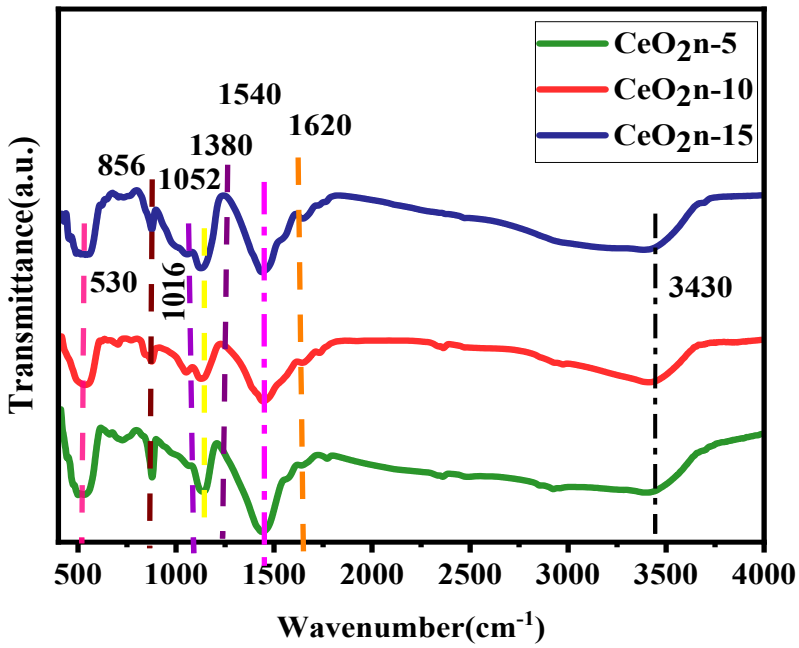

Fig. 4. FTIR diagram of CeO_2n at three different concentrations.

nanoparticles (CeO_2n), presenting a greener and more sustainable alternative to conventional chemical methods. Panahi-Kalamuei, Mokhtar, et al. also attained these outcomes [18]. Arumugam, Ayyakannu, and colleagues focus on the synthesis of CeO_2n utilizing the leaf extract of Gloriosa superba L [19]. Aseyd Nezhad, et al. concentrate on the generation of CeO_2n via Origanum majorana L. leaf extract [20]. Extracts from the procera flower [21], aloe vera [22], Acorus calamus [23], Azadirachta indica [24], banana peel [25], and Citrus nobilis Lour. Peel [26] serve as examples utilized in the production of CeO_2n.

3.2. Fourier transform infrared spectroscopy (FTIR)

Figure 4 presents the Fourier Transform Infrared (FTIR) spectra of CeO_2n at varying extract concentrations, analyzed within the 400-4000 cm^{-1} range. Despite the different concentrations, the spectra exhibit largely consistent peak positions, suggesting that the extract quantity does not significantly alter the fundamental chemical bonds present. The band observed at 3430 cm^{-1} is related to the vibrations of the O-H groups [27]. The bands at 1620 cm^{-1} and 11540 cm^{-1} are attributed to the C=O stretching of the amide group. The most prominent peak corresponds to the robust C-H vibrational bond detected at 1380 cm^{-1}. In addition, a peak corresponding to the C-O alcohol group bond was observed at 1052 cm^{-1} [28, 29]. Notably, the FTIR spectrum of the *Laurus nobilis* extract exhibits a characteristic peak at 1016 cm^{-1}, which aligns with previously reported findings [30]. Furthermore, the absorption band observed at ca. 530 cm^{-1} can be assigned to the Ce–O stretching vibration of fluorite CeO_2 lattice, which is consistent with the literature report [31]. In addition, Ce–O–C bonding, arising from the interaction between CeO_2n and organic compounds from the plant extract, is proven at 856 cm^{-1} In addition, although biomolecules from the *Laurus nobilis* extract initially bind to cerium ions and nanoparticle surfaces during synthesis, they do not remain on the final product. The samples were calcined at 600 °C, which leads to the complete thermal decomposition and removal of organic compounds [32]. Nevertheless, the transient binding of phytochemicals during the synthesis stage plays a crucial role in controlling particle nucleation, stabilization, and growth. As reported in previous studies, this temporary interaction can have a lasting effect on nanoparticle structure even after the organic species are eliminated by high-temperature treatment [33]. These results suggest that the *Laurus nobilis* extract plays a critical role in capping and stabilizing the CeO_2n during synthesis. The consistent peak positions across different extract concentrations indicate

that the extract primarily influences nanoparticle formation without significantly altering their chemical composition.

3.3. Field emission scanning electron microscope (FESEM)

Figure 5 showcases the morphological characteristics of CeO_2n at three different concentrations of *laurus nobilis* extract, as seen through FESEM. The images show that the nanoparticles take on quasi-spherical shapes and form nanorods. The images demonstrate a heterogeneous particle size distribution within each sample, indicating that the *Laurus nobilis* extract influences not only the formation of the nanoparticles but also the resulting particle size and shape. The estimation of the average diameter of nanoparticles is conducted through the application of the log-normal distribution equation [34].

$$f(D)=\left(\frac{1}{\delta D\sqrt{2\Pi}}\right)exp\left[-\frac{ln^2\left(\frac{D}{D_0}\right)}{2\delta^2}\right] \quad (4)$$

$$\langle D\rangle = D_0 exp\left(\frac{\delta^2}{2}\right) \quad (5)$$

$$\delta_D = \langle D\rangle\left[exp\left(\delta^2-1\right)\right]^{\frac{1}{2}} \quad (6)$$

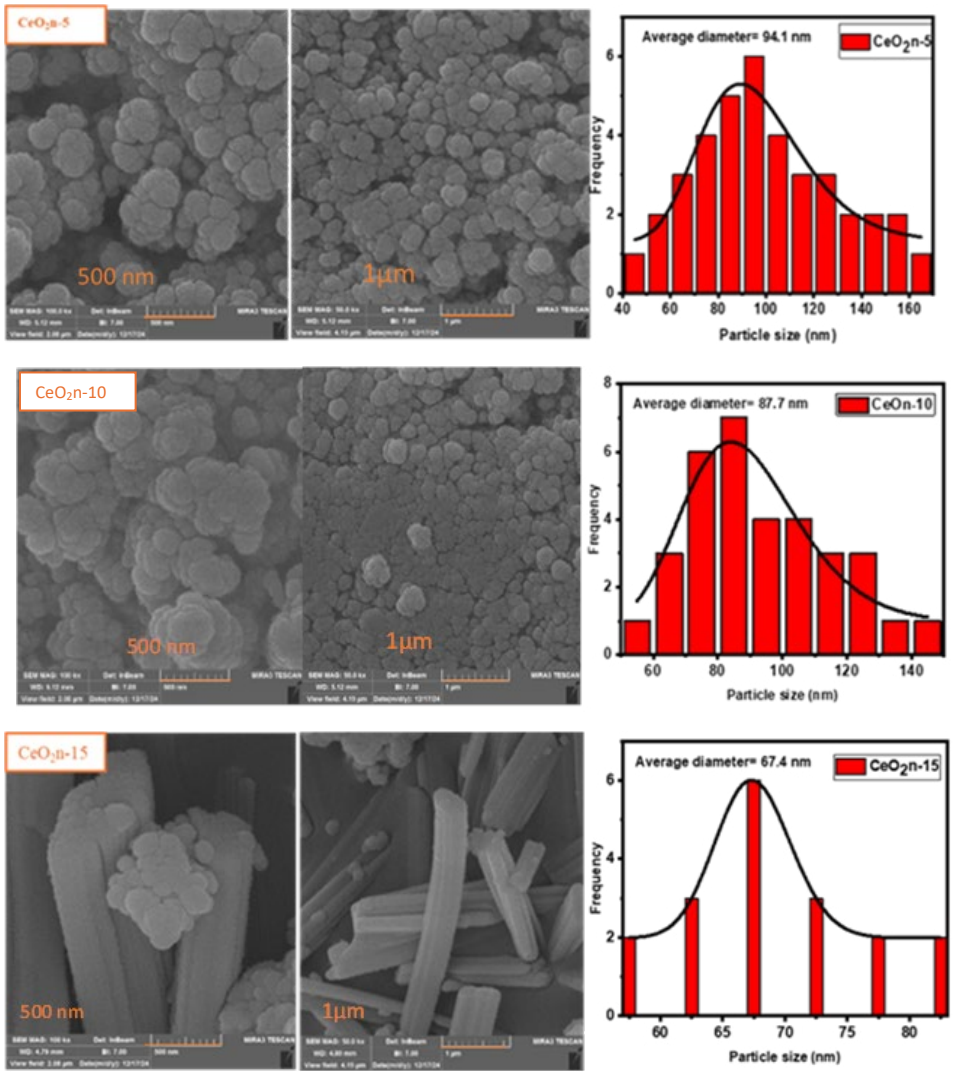

Fig. 5. FESEM images at 1 µm and 500 nm scales for three different CeO_2n samples. Accompanying histograms are provided for each sample.

The parameters D (indicates the diameter of nanoparticle) and δ_0 (is the standard deviation of ln *D*) were obtained from equations 3-5. Additionally, these equations were utilized for data calibration. The synthesis of CeO_2n using *Laurus nobilis* extract demonstrated a clear dependence on the concentration of the extract. As the extract concentration increased from 5 mL to 15 mL, the mean diameter of the nanoparticles decreased significantly from 94.1 nm to 67.4 nm. This reduction in particle size can be attributed to several factors inherent to green synthesis processes. At higher extract concentrations, the abundance of bioactive compounds (such as polyphenols, flavonoids, and other phytochemicals) enhances the efficiency of nucleation by facilitating rapid reduction of metal ions. Additionally, the increased availability of capping agents stabilizes the nanoparticles, preventing their aggregation and thereby limiting their growth. This inverse relationship between extract concentration and nanoparticle size has been widely observed in green synthesis studies, underscoring the critical role of extract concentration in modulating nanoparticle morphology and dimensions [15].

3.4. UV-Vis analysis

Figure 6 (a) presents the UV-Vis absorption spectra of the synthesized CeO_2n across three samples, CeO_2n-5, CeO_2n-10, and CeO_2n-15, with all exhibiting a prominent absorption peak near 300 nm, a blue shift compared to the documented CeO_2n absorption peak at 341 nm [32]. The band gap energies, for varying extract concentrations, were calculated using the Tauc equation [35]:

$$(\alpha h\nu)^2 = k(h\nu - E_g) \quad (7)$$

Here, the symbol α represents the extinction coefficient, E_g is the energy gap, the constant (k) represents different values depending on the specific (possible) transition, and hν is the energy of a photon. Figure 6b shows a plot of (αhν)1/2 versus photon energy (hν). The band gap values for CeO_2n-5, CeO_2n-10, and CeO_2n-15 were determined to be 1.5, 1.75, and 2.25 eV, respectively, demonstrating an inverse relationship between nanoparticle size and band gap energy, consistent with previously reported observations [34, 35]. Specifically, as the particle size decreases (from CeO_2n-5 to CeO_2n-15), the band gap energy increases due to quantum confinement effects, which restrict the movement of electrons and enhance the energy required for electronic transitions. The observed variation in band gap energy highlights the significant influence of *Laurus nobilis* extract concentration on the structural properties of the nanoparticles. Higher extract concentrations lead to smaller particle sizes, thereby increasing the band gap energy. This finding underscores the critical role of synthesis conditions in tailoring the optical and electronic properties of CeO_2n for specific applications, such as photocatalysis and optoelectronics.

3.5. Assessment of photocatalytic effectiveness

Photocatalytic degradation of methyl orange was investigated to evaluate the efficiency of CeO_2n synthesized using varying concentrations of *Laurus nobilis* extract. A 15 ppm solution of methyl orange was prepared by dissolving 0.0015

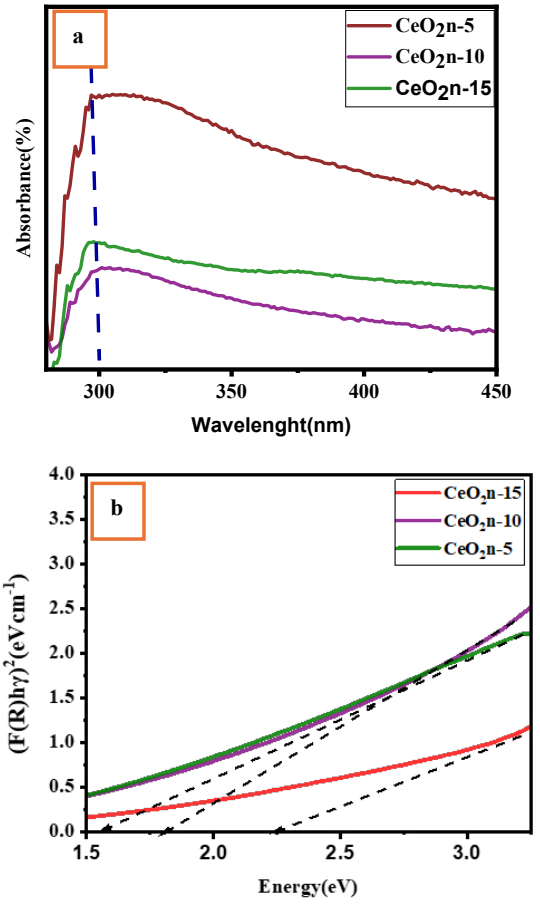

Fig. 6. (a) Ultraviolet-Visible (UV-Vis) spectrum of CeO_2n synthesized using *laurus nobilis* extract. (b) Diagram illustrating the band gap of three samples of CeO_2n.

g of the dye in 100 mL of deionized water. The solution was stirred in the dark for 30 minutes to ensure adsorption-desorption equilibrium between the dye and the nanoparticle surface, thereby enhancing the accuracy of subsequent photocatalytic measurements. The pH of the dye solution was adjusted to approximately pH = 7 and maintained constant throughout the photocatalytic experiments. For the photocatalytic experiments, 0.0026 g of each CeO_2n sample (CeO_2n-5, CeO_2n-10, and CeO_2n-15) was dispersed in 50 mL of the methyl orange solution. The UV-Vis absorption spectra of the solutions were recorded at 30-minute intervals under UV irradiation. As shown in Figure 7, the gradual decrease in the characteristic absorption peak of methyl orange at around 464 nm with increasing irradiation time indicates the progressive breakdown of the azo chromophore, confirming effective photocatalytic degradation. The relative concentration of methyl orange (C/C_0) was calculated using the ratio of absorbance at time t (A_t) to the initial absorbance (A_0), assuming a linear relationship between absorbance and concentration according to the Beer–Lambert law. Accordingly, the plots of C/C_0 and $\ln(C/C_0)$ versus irradiation time (Figure 8) were directly derived from the absorption data shown in Figure 7. Minor deviations between absorbance trends and kinetic plots may arise from light scattering effects and intermediate degradation products formed during the reaction. The gradual decrease in the absorption peak intensity over time confirmed the effective degradation of methyl orange by the CeO_2n. The efficiency of photocatalytic degradation is influenced by several key factors, including pH levels, dye concentration, catalyst dosage, and the structural and morphological characteristics of the nanoparticle surface [36]. Among these, the role of *Laurus nobilis* extract concentration during synthesis was particularly significant, as it directly affected the size, shape, and surface properties of the nanoparticles, thereby influencing their photocatalytic performance. The degradation efficiencies of the nanoparticles were calculated using Equation (8):

$$\eta = \frac{C_t - C_0}{C_0} \times 100 \quad (8)$$

where C_0 represents the initial dye concentration, and C_t represents the concentration of dye at a specific time t. The results revealed degradation efficiencies of 96.5%, 47.5%, and 77.3% for CeO_2n-5, CeO_2n-10, and CeO_2n-15, respectively. Notably, CeO_2n-5

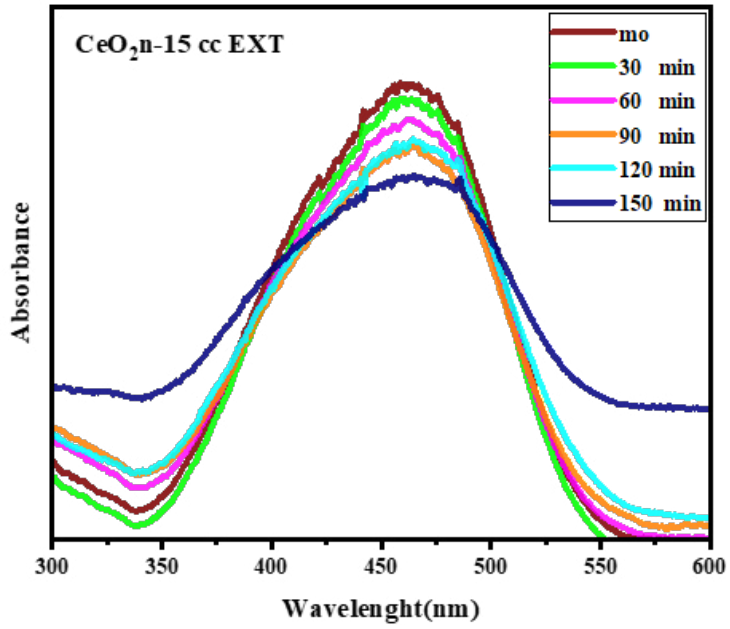

Fig. 7. Diagram of absorption by wavelength at different times related to CeO_2n with three concentrations of laurus nobilis extract

exhibited superior photocatalytic activity, achieving a significantly higher degradation rate compared to the other samples. With increasing *Laurus nobilis* extract concentration, the crystallite size of CeO_2 nanoparticles decreases; however, photocatalytic performance does not follow a monotonic trend. The CeO_2–15 sample exhibits lower photocatalytic efficiency despite its smaller size. This behavior can be attributed to excessive extract-mediated growth, which leads to the formation of rod-like structures and partial aggregation, thereby reducing the number of effective surface-active sites. Furthermore, high extract concentration can disturb the optimal Ce^{3+}/Ce^{4+} redox balance and enhance electron–hole recombination, which suppresses photocatalytic activity. Increased light scattering from elongated structures also lowers effective photon absorption [37]. These findings indicate the existence of an optimal extract concentration, as observed for CeO_2–5, at which charge separation and surface reactivity are maximized, resulting in superior photocatalytic performance [38]. Figure 7 illustrates the percentage of color degradation relative to the baseline state (pure methyl orange without a photocatalyst). CeO_2n-5 demonstrated rapid color reduction during both the initial 60 minutes and the final 30 minutes of the experiment, underscoring its superior photocatalytic efficiency. Furthermore, Figure 8 presents the correlation between $\ln(C/C_0)$ and the duration of UV irradiation, confirming pseudo-first-order kinetics for the degradation process, which is shown in equation 8. The linear relationship can be expressed through the following equation (9)[39].

$$\ln\left(\frac{C_t}{C_0}\right) = ln\left(\frac{A_t}{A_0}\right) = kt \quad (9)$$

In this regard, replacing optical absorbance (A) with concentration (Ct) denotes the dye concentration at a specific time interval, where k represents the velocity of reaction [40]. The higher the k, the faster the degradation rate increases linearly [41]. These findings highlight the potential of CeO_2n synthesized using *Laurus nobilis* extract as an effective and eco-friendly photocatalyst for wastewater treatment applications.

3.6. Antioxidant Activity of Green Synthesized CeO_2n

The antioxidant potential of green-synthesized CeO_2n was evaluated in vitro through the DPPH (stands for 2,2-diphenyl-1-picrylhydrazyl) radical scavenging assay. DPPH is a stable free radical characterized by a deep purple color and displays maximum absorbance at 517 nm. The antioxidant capacity is assessed by monitoring the decrease in this characteristic absorbance, reflecting the scavenging of DPPH radicals. Antioxidant analysis for a 5 mL sample of *Laurus nobilis* extract at different concentrations is shown in Figure 8. Results demonstrated that the radical quenching activity of CeO_2n increased in a concentration-dependent manner, achieving a maximal inhibition of 75.5% at 17.6 µg/mL (Fig. 9). In comparison, the standard antioxidant, ascorbic acid, exhibited 89.9% inhibition at the same concentration and was used as a control to benchmark the antioxidant efficacy. The observed scavenging

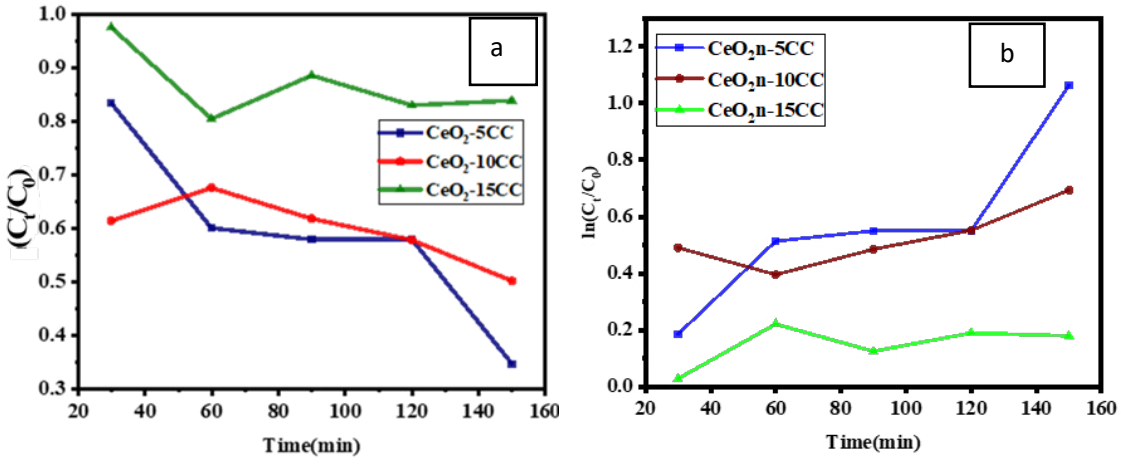

Fig. 8. a) $\frac{C_t}{c_0}$ diagram and b) $\ln\frac{C_t}{c_0}$ diagram of CeO_2n..

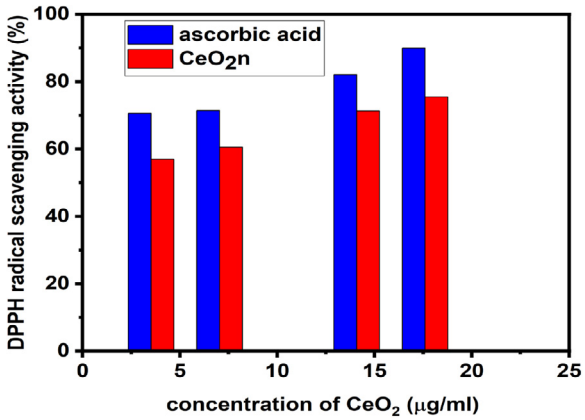

Fig. 9. DPPH radical scavenging action of CeO_2n nanoparticles and ascorbic acid.

Table 1. compares the CeO_2n synthesis via different extracts with our study and reports their results.

Method	Plant extract	Particle size (nm)	Photocatalyst activity	Anti-oxidant activity $\left(\mu g/ml\right)$	Ref
Chemically & Green synthesis	*Solanum nigrum leaf*	20	78.14% 94.58%	50	[42]
Green synthesis	Sapodilla fruit peel	10 ± 1.5	90%	--------	[43]
Green synthesis	*abelmoschus esculentus*	30	--------	9.36 &15.47	[44]
Green synthesis	*Laurus nobilis*	15.35 16.1 21.11	96.5% 47.5% 77.3%	75.5	This study

activity is attributed to electron transfer from oxygen atoms on the nanoparticle surface to the nitrogen atoms of DPPH molecules, resulting in the formation of more stable radical species. Prior research confirms that various metal nanoparticles possess significant free radical scavenging abilities, primarily due to their high surface-to-volume ratios. For instance, zinc oxide nanoparticles have also demonstrated enhanced antioxidant action at elevated concentrations. Notably, recent studies highlight CeO_2n as promising antioxidant agents. Specifically, CeO_2n synthesized using *Laurus nobilis* extract have shown superior antioxidant performance, underscoring their potential utility in biomedical applications.

Challenges in Photocatalytic Applications

· Limited Visible Light Absorption

CeO_2 has a wide band gap (~3.2 eV), which restricts its activity mostly to UV light. Enhancing visible light responsiveness remains a key hurdle[45].

· Charge Carrier Recombination

Rapid recombination of photo-generated electrons and holes reduces photocatalytic efficiency. Strategies like doping or heterojunction formation are often needed to mitigate this [46].

• Surface Area and Morphology Control

Green synthesis methods can lead to inconsistent particle sizes and morphologies, affecting surface area and catalytic activity[47].

· Stability Under Reaction Conditions

CeO_2 NPs may undergo structural changes or aggregation during photocatalytic reactions, reducing their long-term effectiveness[48].

Challenges in Antioxidant Applications

· Reactive Oxygen Species (ROS) Regulation

While CeO_2 can scavenge ROS due to its redox cycling between Ce^{3+} and Ce^{4+}, maintaining this balance in biological environments is complex and can vary with pH and ionic strength.

· *Biocompatibility and Toxicity*

Although green synthesis enhances biocompatibility, the long-term effects of CeO_2 NPs in biological systems remain under investigation. Dose-dependent cytotoxicity has been observed in several studies [49].

· *Reproducibility and Scalability*

Plant-mediated synthesis can be difficult to standardize due to variations in extract composition, affecting reproducibility and scalability for industrial or clinical use.

· *Interaction with Biomolecules*

CeO_2 NPs may interact unpredictably with proteins, enzymes, or cellular membranes, potentially altering their antioxidant behavior or triggering immune responses.

Conclusion

In this study, the effect of *Laurus nobilis* extract concentration on (CeO_2n) was investigated. This is the first time that *L. nobilis* extract has been used to produce green nanoparticles, and its antioxidant and photocatalytic properties have been evaluated. The findings of this study demonstrate that *Laurus nobilis* extract provides a cost-effective, rapid, and eco-friendly method for synthesizing cerium oxide nanoparticles (CeO_2n). The biomolecules present in the extract play a critical role in both capping and stabilizing the nanoparticles during synthesis. XRD analysis confirmed the crystalline structure of CeO_2n, consistent with the cubic fluorite phase (JCPDS card number 8436-089-01), while FESEM revealed quasi-spherical and nanorod morphologies. UV-Vis spectroscopy indicated an absorption peak near 300 nm, with band gap energies inversely related to nanoparticle size. Photocatalytic degradation of methyl orange yielded efficiencies of 96.5%, 47.5%, and 77.3% for CeO_2n-5, CeO_2n-10, and CeO_2n-15, respectively. These results highlight the significant impact of extract concentration on nanoparticle properties and photocatalytic performance. The incorporation of plant extract in the synthesis of CeO_2n significantly enhanced their antioxidant activity. This suggests that bio-mediated synthesis methods can improve the free radical scavenging efficiency of CeO_2n for potential biomedical uses.

References

[1] S. Bayda, M. Adeel, T. Tuccinardi, M. Cordani, F. Rizzolio, The history of nanoscience and nanotechnology: from chemical–physical applications to nanomedicine. Molecules 25 (2019) 112. https://doi.org/10.3390/molecules25010112.

[2] K. Ali, T. Cherian, S. Fatima, Q. Saquib, M. Faisal, A.A. Alatar, J. Musarrat, A.A. Al-Khedhairy, Role of solvent system in green synthesis of nanoparticles. In Green synthesis of nanoparticles: applications and prospects Singapore: Springer Singapore (2020) 53-74. https://doi.org/10.1007/978-981-15-5179-6_3.

[3] P. Iqbal, J. A. Preece, P. M. Mendes, Nanotechnology: the "top-down" and "bottom-up" approaches, Supramolecular chemistry: from molecules to nanomaterials (2012). https://doi.org/10.1002/9780470661345.smc195.

[4] R. Zarei Moghadam, M. H. Ehsani, H. Rezagholipour Dizaji, M. R. Sazideh, Thickness Dependence of Structural and Optical Properties of CdTe Films, Iran. J. Mater. Sci. Eng. 15 (2018). 10.22068/ijmse.15.3.21.

[5] C. Mallikarjunaswamy, J. S. Vidya, H. N. Deepakumari, G. Nagaraju, M. A. Sangamesha, V. Lakshmi Ranganatha, Larvicidal and antimicrobial activity of zinc oxide nanoparticles synthesized from rain tree pod aqueous extract, Mater. Today: Proc. 62 (2022) 5083-5086. https://doi.org/10.1016/j.matpr.2022.02.422.

[6] C. Mallikarjunaswamy, V. Lakshmi Ranganatha, R. Ramu, Udayabhanu, G. Nagaraju, Facile microwave-assisted green synthesis of ZnO nanoparticles: application to photodegradation, antibacterial and antioxidant, J. Mater. Sci. 31 (2020) 1004-1021. https://doi.org/10.1007/s10854-019-02612-2.

[7] K. B. Narayanan, N. Sakthivel, Green synthesis of biogenic metal nanoparticles by terrestrial and aquatic phototrophic and heterotrophic eukaryotes and biocompatible agents, Adv. Colloid Interface Sci. 169 (2011) 59-79. https://doi.org/10.1016/j.cis.2011.08.004.

[8] J. Gagnon, K. M. Fromm, Toxicity and protective effects of cerium oxide nanoparticles (nanoceria) depending on their preparation method, particle size, cell type, and exposure route, Eur. J. Inorg. Chem. 2015 (2015) 4510-4517. https://doi.org/10.1002/ejic.201500643.

[9] M. Nadeem, R. Khan, K. Afridi, A. Nadhman, S. Ullah, S. Faisal, Z. Ul Mabood, C. Hano, B. Haider Abbasi, Green synthesis of cerium oxide nanoparticles (CeO_2 NPs) and their antimicrobial applications: a review, Int J Nanomedicine. (2020) 5951-5961. https://doi.org/10.2147/IJN.S255784.

[10] K. N. Lokesh, R. R. Sivakiran, Biological methods of dye removal from textile effluents-A review, J. Biochem. Technol. 3 (2014) 177-180.

[11] C. R. Chenthamarakshan, K. Rajeshwar, E. J. Wolfrum, Heterogeneous photocatalytic reduction of Cr (VI) in UV-irradiated titania suspensions: effect of protons, ammonium ions, and other interfacial aspects, Langmuir. 16 (2000) 2715-2721. https://doi.org/10.1021/la9911483.

[12] S. Vijayakumar, B. Vaseeharan, B. Malaikozhundan, M. Shobiya, Laurus nobilis leaf extract mediated green synthesis of ZnO nanoparticles: Characterization and biomedical applications, Biomed Pharmacother. 84 (2016) 1213-1222. https://doi.org/10.1016/j.biopha.2016.10.038.

[13] H. Samadi, R. Zarei Mohgadam, M. Gholipour Shahraki, Green synthesis of ZnO nanoparticles, photocatalyst activity and its biomedical applications: A review, Mater. Chem. Phys. (2025) 131161. https://doi.org/10.1016/j.

matchemphys.2025.131161.

[14] S. L. Pirard, C. M. Malengreaux, D. Toye, B. Heinrichs, How to correctly determine the kinetics of a photocatalytic degradation reaction?, Chem. Eng. J. 249 (2014) 1-5. https://doi.org/10.1016/j.cej.2014.03.088.

[15] C. A. Soto-Robles, P. A. Luque, C. M. Gómez-Gutiérrez, O. Nava, A. R. Vilchis-Nestor, E. Lugo-Medina, R. Ranjithkumar, A. Castro-Beltrán, Study on the effect of the concentration of Hibiscus sabdariffa extract on the green synthesis of ZnO nanoparticles, Results Phys. 15 (2019) 102807. https://doi.org/10.1016/j.rinp.2019.102807.

[16] U. Holzwarth, N. Gibson, The Scherrer equation versus the'Debye-Scherrer equation, Nat. Nanotechnol. 6 (2011) 534-534. https://doi.org/10.1038/nnano.2011.145.

[17] A. O. Bokuniaeva, A. S. Vorokh, Estimation of particle size using the Debye equation and the Scherrer formula for polyphasic TiO_2 powder, J. Phys. Conf. Ser. 1410 (2019) 012057. 10.1088/1742-6596/1410/1/012057.

[18] M. Panahi-Kalamuei, S. Alizadeh, M. Mousavi-Kamazani, M. Salavati-Niasari, Synthesis and characterization of CeO_2 nanoparticles via hydrothermal route, J. Ind. Eng. Chem. 21 (2015) 1301-1305. https://doi.org/10.1016/j.jiec.2014.05.046.

[19] A. Arumugam, C. Karthikeyan, A. Syedahamed Haja Hameed, K. Gopinath, S. Gowri, V. Karthika, Synthesis of cerium oxide nanoparticles using Gloriosa superba L. leaf extract and their structural, optical and antibacterial properties, Mater. Sci. Eng. C. 49 (2015) 408-415. https://doi.org/10.1016/j.msec.2015.01.042.

[20] S. Aseyd Nezhad, A. Es-haghi, M. Homayouni Tabrizi, Green synthesis of cerium oxide nanoparticle using Origanum majorana L. leaf extract, its characterization and biological activities, Appl. Organomet. Chem. 34 (2020) e5314. https://doi.org/10.1002/aoc.5314.

[21] A. Muthuvel, M. Jothibas, V. Mohana, C. J. I. C. C. Manoharan, Green synthesis of cerium oxide nanoparticles using Calotropis procera flower extract and their photocatalytic degradation and antibacterial activity, Inorg. Chem. Commun. 119 (2020) 108086. https://doi.org/10.1016/j.inoche.2020.108086.

[22] D. Dutta, R. Mukherjee, M. Patra, M. Banik, R. Dasgupta, M. Mukherjee, T. Basu, Green synthesized cerium oxide nanoparticle: A prospective drug against oxidative harm, Colloids Surf. B Biointerfaces. 147 (2016) 45-53. https://doi.org/10.1016/j.colsurfb.2016.07.045.

[23] M. Altaf, S. Manoharadas, M. Tarique Zeyad, Green synthesis of cerium oxide nanoparticles using Acorus calamus extract and their antibiofilm activity against bacterial pathogens, Microsc Res Tech. 84 (2021) 1638-1648. https://doi.org/10.1002/jemt.23724.

[24] N. Masood, M. Atif Irshad, R. Nawaz, T. Abbas, M. A. Abdel-Maksoud, W. H. AlQahtani, H. AbdElgawad, M. Rizwan, A. HA Abeed, Green synthesis, characterization and adsorption of chromium and cadmium from wastewater using cerium oxide nanoparticles; reaction kinetics study, J. Mol. Struct. 1294 (2023) 136563. https://doi.org/10.1016/j.molstruc.2023.136563.

[25] A. Miri, H. Beiki, A. Najafidoust, M. Khatami, M. Sarani, Cerium oxide nanoparticles: green synthesis using Banana peel, cytotoxic effect, UV protection and their photocatalytic activity, Bioprocess Biosyst. Eng. 44 (2021) 1891-1899. https://doi.org/10.1007/s00449-021-02569-9.

[26] G. E. Putri, A. Labanni, S. Arief, P. Dafriani, I. Yulia Darma, S. Handayani, N. Jaffar, M. Mahmud, A. Hafizullah Ritonga, Green synthesis of cerium oxide nanoparticles using Citrus nobilis Lour. Peel extract and evaluation of their potential as antibacterial and antioxidant agents, Case Stud. Chem. Environ. Eng. 11 (2025) 101062. https://doi.org/10.1016/j.cscee.2024.101062.

[27] A. R. Rajan, V. Vilas, A. Rajan, A. John, D. Philip, Synthesis of nanostructured CeO_2 by chemical and biogenic methods: optical properties and bioactivity, Ceram. Int. 46 (2020) 14048-14055. https://doi.org/10.1016/j.ceramint.2020.02.204.

[28] M. Farahmandjou, M. Zarinkamar, T. P. Firoozabadi, Synthesis of Cerium Oxide (CeO_2) nanoparticles using simple CO-precipitation method, Rev. Mex. Fis. 62 (2016) 496-499.

[29] S. N. Naidi, F. Khan, A. Ling Tan, M. Hilni Harunsani, Y-M. Kim, M. Mansoob Khan, Photoantioxidant and antibiofilm studies of green synthesized Sn-doped CeO_2 nanoparticles using aqueous leaf extracts of Pometia pinnata, New J Chem. 45 (2021) 7816-7829. https://doi.org/10.1039/D1NJ00416F.

[30] E. A. Araújo, N. José de Andrade, L. Henrique Mendes da Silva, A. Fernandes de Carvalho, C. Antônio de Sá Silva, A. Mota Ramos, Control of microbial adhesion as a strategy for food and bioprocess technology, Food Bioprocess Technol. 3 (2010) 321-332. https://doi.org/10.1007/s11947-009-0290-z.

[31] Y. W. Hartati, S. Nur Topkaya, S. Gaffar, H. H. Bahti, A. E. Cetin, Synthesis and characterization of nanoceria for electrochemical sensing applications, RSC Adv. 11 (2021) 16216-16235. 10.1039/D1RA00637A.

[32] S. Pansambal, R. Oza, S. Borgave, A. Chauhan, P. Bardapurkar, S. Vyas, S. Ghotekar, Bioengineered cerium oxide (CeO_2) nanoparticles and their diverse applications: a review, Appl. Nanosci. 13 (2023) 6067-6092. https://doi.org/10.1007/s13204-022-02574-8.

[33] M. Jothibas, E. Paulson, A. Mathivanan, S. Srinivasan, K. Senthil Kannan, Biomolecules influences on the physiochemical characteristics of ZnO nanoparticles and its enhanced photocatalysis under solar irradiation, Nanotechnol. Environ. Eng. 8 (2023) 511-533. https://doi.org/10.1007/s41204-023-00310-3.

[34] R. Zarei Moghadam, H. Rezagholipour Dizagi, H. Agren, M. H. Ehsani, Understanding the effect of Mn^{2+} on Yb^{3+}/Er^{3+} co-doped $NaYF_4$ upconversion and obtaining the optimal combination of these tridoping, Sci. Rep. 13 (2023) 17556. https://doi.org/10.1038/s41598-023-44947-1.

[35] J. Klein, L. Kampermann, B. Mockenhaupt, M. Behrens, J. Strunk, G. Bacher, Limitations of the Tauc plot method, Adv. Funct. Mater. 33 (2023) 2304523. https://doi.org/10.1002/adfm.202304523.

[36] M. Naushad, S. Rajendran, E. Lichtfouse, Green photocatalysts, First ed. Cham, Switzerland: Springer International Publishing 2020. https://doi.org/10.1007/978-3-030-15608-4.

[37] D. Li, H. Song, X. Meng, T. Shen, J. Sun, W. Han, X. Wang, Effects of particle size on the structure and photocatalytic performance by alkali-treated TiO_2, J. Nanomater. 10 (2020) 546. https://doi.org/10.3390/nano10030546.

[38] F. Pellegrino, L. Pellutiè, F. Sordello, C. Minero, E. Ortel, V-D. Hodoroaba, V. Maurino, Influence of agglomeration

and aggregation on the photocatalytic activity of TiO_2 nanoparticles, Appl. Catal. B: Environ. 216 (2017) 80-87. https://doi.org/10.1016/j.apcatb.2017.05.046.

[39] N. Assad, A. Abbas, M. Fayyaz ur Rehman, M. Naeem-ul-Hassan, Photo-catalytic and biological applications of phyto-functionalized zinc oxide nanoparticles synthesized using a polar extract of Equisetum diffusum D, RSC Adv. 14 (2024) 22344-22358. https://doi.org/10.1039/D4RA03573A.

[40] A. B. Siddique, M. A. Shaheen, A. Abbas, Y. Zaman, M. A. Bratty, A. Najmi, A. Hanbashi M. Mustaqeem, H. A. Alhazmi, Z. ur Rehman, K. Zoghebi, Thermodynamic and kinetic insights into azo dyes photocatalytic degradation on biogenically synthesized ZnO nanoparticles and their antibacterial potential, Heliyon. 10 (2024). https://doi.org/10.1016/j.heliyon.2024.e40679.

[41] S. Li, J. Hu, Photolytic and photocatalytic degradation of tetracycline: Effect of humic acid on degradation kinetics and mechanisms, J. Hazard. Mater. 318 (2016) 134-144. https://doi.org/10.1016/j.jhazmat.2016.05.100.

[42] A. Muthuvel, M. Jothibas, C. Manoharan, S. Johnson Jayakumar, Synthesis of CeO_2-NPs by chemical and biological methods and their photocatalytic, antibacterial and in vitro antioxidant activity, Res. Chem. Intermed. 46 (2020). 10.1007/s11164-020-04115-w.

[43] D. Ayodhya, A. Ambala, G. Balraj, M. Pradeep Kumar, P. Shyam, Green synthesis of CeO_2 NPs using Manilkara zapota fruit peel extract for photocatalytic treatment of pollutants, antimicrobial, and antidiabetic activities, Results Chem. 4 (2022) 100441. https://doi.org/10.1016/j.rechem.2022.100441.

[44] A. Ahmad, M. Sufyan Javed, S. Khan, T. Mazyad Almutairi, A. AA Mohammed, R. Luque, Green synthesized Ag decorated CeO_2 nanoparticles: Efficient photocatalysts and potential antibacterial agents, Chemosphere 310 (2023) 136841. https://doi.org/10.1016/j.chemosphere.2022.136841.

[45] A. E. Herzog, T. J. Michael, A. D. Dunkelberger, M. D. Johannes, D. R. Rolison, P. A. DeSario, T. G. Novak, Nanostructured CeO_2 photocatalysts: optimizing surface chemistry, morphology, and visible-light absorption, Nanoscale 16 (2024) 9659-9679. https://doi.org/10.1039/D4NR00676C.

[46] E. Spurio, J. Stefano Pelli Cresi, G. Ammirati, S. Pelatti, A. Paladini, S. D'Addato, S. Turchini, P. O'Keeffe, D. Catone, P. Luches. Injecting electrons into CeO_2 via photoexcitation of E. Au nanoparticles, ACS photonics 10 (2023) 1566-1574. https://doi.org/10.1021/acsphotonics.3c00184.

[47] B. Xu, Q. Zhang, S. Yuan, M. Zhang, T. Ohno, Morphology control and characterization of broom-like porous CeO_2, Chem. Eng. J. 260 (2015) 126-132. https://doi.org/10.1016/j.cej.2014.09.001.

[48] C. Li, Y. Sun, I. Djerdj, P. Voepel, C-C. Sack, T. Weller, R. Ellinghaus, J. Sann, Y. Guo, B. M. Smarsly, H. Over, Shape-controlled CeO_2 nanoparticles: stability and activity in the catalyzed HCl oxidation reaction, ACS Catal. 7 (2017) 6453-6463. https://doi.org/10.1021/acscatal.7b01618.

[49] Y. Ma, P. Li, L. Zhao, J. Liu, J. Yu, Y. Huang, Y. Zhu, Z. Li, R. Zhao, S. Hua, Y. Zhu, Size-dependent cytotoxicity and reactive oxygen species of cerium oxide nanoparticles in human retinal pigment epithelia cells, Int J Nanomedicine. (2021) 5333-5341. https://doi.org/10.2147/IJN.S305676.